Spring 5-13-2023

Synthesis and Characterization of Sodium Cathode Materials

He Zhou

WASHINGTON UNIVERSITY IN ST. LOUIS

McKelvey School of Engineering
Department of Mechanical Engineering & Materials Science

Thesis Examination Committee:
Peng Bai, Chair
Sanghoon Bae
Xianglin Li

Synthesis and Characterization of Sodium Cathode Materials

by
He Zhou

A thesis presented to
the McKelvey School of Engineering
of Washington University in
partial fulfillment of the
requirements for the degree
of Master of Science

May 2023
St. Louis, Missouri

Table of Contents

List of Figures

Acknowledgments

Time flies and two-year of my Master's program studies finally reach an end. I am extremely grateful for being able to study at Washington University in St. Louis. This unique experience that I will certainly treasure in my heart. Therefore, I am writing this acknowledgment to thank all the people who supported me during this program.

First and foremost, I would like to express my gratitude to my advisor Dr. Peng Bai. I'm so grateful to him for giving me a chance to research batteries in his lab. Under his guidance, I have gained plenty of experience relevant to energy research, which has strengthened my determination to continue my exploration in this field. He is passionate about research and always has a unique perspective. He cares deeply about the development of his students, always sharing his knowledge and resources selflessly. Thank you for believing in me and for being an outstanding mentor.

In addition, I would like to appreciate Dr. Sanghoon Bae, and Dr, Xianglin Li. Thank them for their valuable contribution to my thesis defense. I also want to thank Dr. Sanghoon Bae and Dr. Bryce Sadtler for recommending me to the Ph.D. programs. Their willingness to support me and their kind words and useful suggestions have been invaluable in helping me pursue my academic and career goals.

Moreover, I'm thankful to every Battery Analytical Investigation (BAI) group member. Shubham Agrawal, Bingyuan Ma, Youngju Lee, Poom Sittisomwong, Rajeev Gopal, Penghao Zhang, and Ethan Boutelle, you are the best colleagues I have ever met. Thank you so much for sharing your incredible ideas with me, which greatly benefit me.

Finally, I would like to thank my family, especially my parents, Wenxia Wang, and Hongtao Zhou,

for their unconditional love and support throughout my whole life. I also want to thank Yashi Wang, my closest friend, for supporting me, sharing my joys, and bearing my pains. Her companionship gave me the strength to complete my two-year academic career and provided me with great emotional support.

He Zhou

Washington University in St. Louis

May 2023

Dedicated to my family and friends.

ABSTRACT OF THE THESIS

Synthesis and Characterization of Sodium Cathode Materials

by

He Zhou

Master of Science in Materials Science and Engineering

Washington University in St. Louis, 2023

Professor Peng Bai, Chair

As sodium batteries hold great promise as a next-generation energy storage device to replace lithium batteries, the development of sodium battery materials has become increasingly urgent. The current study aims to investigate two potential sodium-ion battery cathode materials, Sodium Vanadium Phosphate, and Sodium Manganese Hexacyanoferrate, optimize the experimental procedures, conduct a systematic analysis of material properties and characterization, and ultimately determine the ideal synthesis conditions for these materials.

In the first part of the study, we focused on optimizing the synthesis of Sodium Vanadium Phosphate. By investigating various synthesis conditions, such as annealing temperature, pressure, ascorbic acid content, and material addition order, the study identified the optimal parameters for achieving high capacity and cyclic stability. We also found the key phenomenon that indicates the high performance of materials. The highest capacity of NVP could reach 96mAh/g at 1C.

In the second part of the study, we investigated two synthesis methods: one with a chelating agent and the other without. For the chelation-free method, we optimized ethanol content, aging time, and washing reagents and achieved the highest capacity of 112 mAh/g at 1C with an ethanol ratio of 1:3, an aging time of 12 hours, and deionized water as the washing solvent. In the chelating agent method, we used tetra-sodium EDTA as the chelating agent and added ascorbic acid as a dissociating agent. This method resulted in a material with a good dispersion system and achieved a capacity of 130 mAh/g at 1C. For future PBA synthesis, we plan to optimize based on this method and expand it to KPBA synthesis as much as possible.

Chapter 1: Introduction

1.1 Background

1.1.1 Development of Batteries

In the face of the increasingly severe energy crisis, the use of clean energy is more conducive to meeting the goal of sustainable development.[1] Clean energy resources, such as wind, solar power, and hydropower, are becoming important ways as we face climate change and the depletion of fossil fuels.[2-5] In this context, batteries have emerged as a promising technology for storing excess energy generated by clean energy resources. Especially, since rechargeable lithium-ion batteries (LIBs) were first commercialized by Sony in 1991, it has revolutionized the energy storage field and continue to dominate in the electronic market, playing a significant role in various applications such as electric vehicles (EVs) and smart portable devices.[5-7] Because of their long recycle life, high gravimetric energy, and high power density, LIBs are considered one of the most efficient energy storage devices with a wide range of applications.[8-12] However, there are still limitations that hinder the further development of LIBs, with their energy density expected to plateau slightly above 300Wh/kg.[13] Furthermore, the growing demand for LIBs in various industries has raised concerns regarding the scarcity of lithium resources in nature.[14] Additionally, the increased demand for lithium-ion batteries in the automotive industry and other sectors may put pressure on the supply chain, leading to potential price hikes and supply shortages.[6,14,15.] Therefore, one of the objectives of developing the next generation of batteries is to find a substitute for lithium.

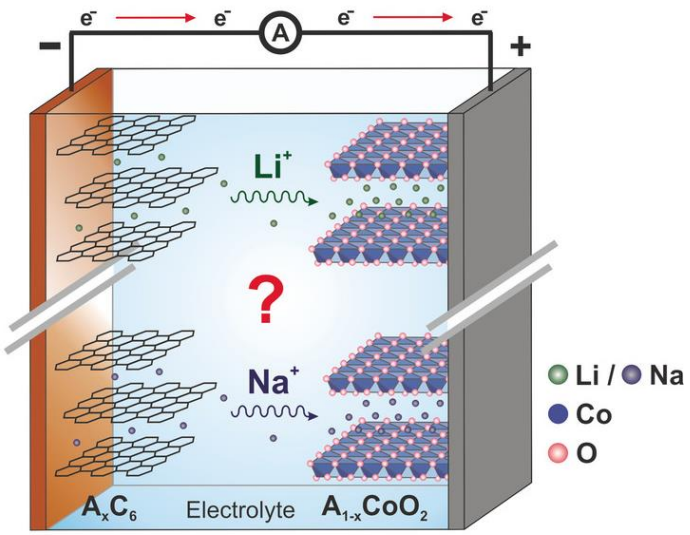

Figure 1.1 The working principle of LIB and SIB.

Sodium-ion batteries (SIBs) have emerged as a promising alternative to LIBs due to their similarity in properties to lithium and the abundance and affordability of sodium resources.[16-18] Figure 1.1 shows the working principle of the LIBs. While the working principle of SIBs is similar to LIBs, the size difference between lithium and sodium contributes to the considerably different electrochemical behavior. These differences lead to challenges in developing high-performance sodium-ion batteries. For example, compared to lithium ions, sodium ions have less desolvation energy, and lower energy density, as well as a higher standard reduction potential of Na^+/Na[19, 20] Ongoing research and development efforts in the field of sodium-ion batteries are aimed at improving their performance and making them a more viable option for energy storage solutions in the future.

Here, we address two promising sodium ion cathode materials, Sodium Vanadium Phosphate (NVP) and Sodium Prussian Blue Analogue (Na-PBA).

1.1.2 Sodium Vanadium Phosphate

NVP is a typical sodium superionic conductor (NASICON) compound, which has extraordinary properties on high Na^+ conductivity, structural stability, and energy density.[21-23] The structure of NVP is shown in Figure 1.2. However, NVP exhibits low intrinsic electronic conductivity (1.63×10^{-6} S/cm), which limits its practical application.[24] In addition, Na^+ has a lower diffusion rate in NVP due to its larger ion radius and molecular weight, resulting in poor performance.[21] To address these issues, several techniques such as carbon coating, particle downsizing, and elemental doping have been employed to enhance the material's performance.[21,24,25]

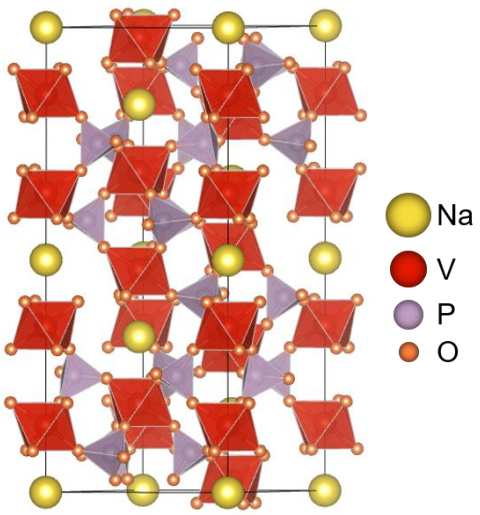

Figure 1.2 The structure of NVP

Carbon coating is a particularly favorable method to improve the NVP's performance because this method not only reduces the diffusion length of Na^+ but also enhances the electron conductivity.[26-28] Jun Chen et al. developed a hydrothermal-assisted sol-gel method to synthesize the NVP@C core-shell structure nanocomposite.[27] They adopted 2 carbon resources, ascorbic acid, and PEG-400, to coat NVP twice. The nanoparticle size was limited to 40nm while preventing agglomeration and producing more

uniform particles. The initial discharge capacity of the as-prepared NVP@C is 104.3 $mA{\cdot}h{\cdot}g^{-1}$ at 0.5 C and 94.9 $mA{\cdot}h{\cdot}g^{-1}$ at 5 C with 96% capacity retention after 700 cycles. Cao's group developed a new design of hierarchical carbon framework wrapped NVP, resulting in a specific capacity that could remarkably reach 115 $mA{\cdot}h{\cdot}g^{-1}$ at 0.2 C and 38 $mA{\cdot}h{\cdot}g^{-1}$ at 500 C.[29] To achieve this, they used chemical vapor deposition (CVD) to create a graphene or carbon nanofiber framework that coated and interconnected the NVP particles. Meanwhile, Yang et.al synthesized the $Na_3V_2(PO_4)_3$/C nanocomposite through the simple pre-reduction and subsequent calcination process.[30] The material, used as the cathode, exhibited the initial discharge capacity of 106 $mA{\cdot}h{\cdot}g^{-1}$ at a current rate of 20 $mA{\cdot}h{\cdot}g^{-1}$.

Elemental doping is considered another efficient way to improve the conductivity of NVP.[31,32,37] Metallic and non-metallic element doping can ultimately increase the electrical conductivity of NVP, although they act on different principles.[33] Mingqi Li et.al utilized dopamine and citric acid as sources of nitrogen and carbon, respectively, to create a double-carbon coated $Na_3V_2(PO_4)_3$/C/NC material.[34] The nitrogen-doped carbon derived from dopamine effectively prevented the growth and agglomeration of $Na_3V_2(PO_4)_3$/C particles. Additionally, it caused an increase in the ionic conductivity due to an increase in the defect density of the carbon layer. Furthermore, the electronic conductivity was improved because of the n-type doping. NVP/C/NC composite cathode exhibits a high initial reversible capacity, 109.2 $mA{\cdot}h{\cdot}g^{-1}$ at 0.2C and 87.2 $mA{\cdot}h{\cdot}g^{-1}$ at a rate up to 20C. Additionally, Shanshan Jiang et.al doped phosphate to NVP@C.[35] Their material shows a specific capacity of 110.6 $mA{\cdot}h{\cdot}g^{-1}$ at 0.5 C and a high capacity retention of 91.2% over 500 cycles at 20 C. Besides the non-metallic doping, Kwon's group doped K^+ to $Na_3V_2(PO_4)_3$/C composite.[36] Since K^+ has a larger ionic

radius, it enlarges the Na^+ diffusion pathway and ensures the doping K-ion hardly attends the electrochemical reaction and finally reaches 110.4 $mA{\cdot}h{\cdot}g^{-1}$ at 0.2C, which is close to the theoretical capacity 117 $mA{\cdot}h{\cdot}g^{-1}$.

1.1.3 Prussian Blue Analog

Prussian blue Analog (PBAs) is a general term for specific compounds that have metal-organic frameworks. We take our material as the example exhibiting the structure below (Figure. 1.3）. The chemical formula of PBA could be expressed as $A_xM[Fe(CN)_6]_y{\cdot}\square_{1-y}{\cdot}nH_2O$ ($0 \leq x \leq 2$, $y < 1$), where A is the alkali-metal ion. M represents the transition-metal ion, usually Co, Fe, and Mn.[38-40]d Fe connects to CN^- to generate the open structure and can carry the A ion in the structure. □ is the vacancy of $M^{'}(CN)_6$, and H_2O is crystal water.[41-43] The addition of some variable-valence transition metal M makes PBA a two-electron-transfer type, which is not only low-cost and easy to synthesize but also has a high theoretical capacity (up to 170. $mA{\cdot}h{\cdot}g^{-1}$).[42]

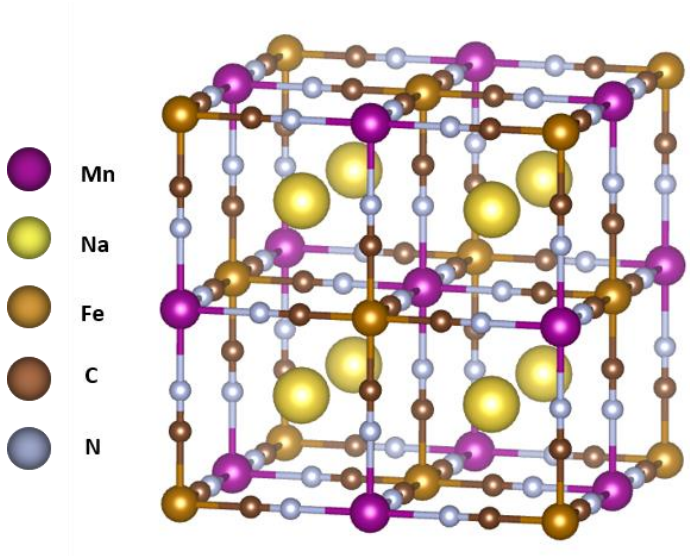

Figure 1.3 The structure of Na-MPBA

According to all PBAs, sodium manganese-based PBA (refer to as MnPBA) becomes the most promising cathode material. In addition to the above-mentioned advantages of PBA, manganese has a large storage capacity in ton earth and is also environmentally friendly.[44] The co-precipitation method is commonly used to synthesize MnPBA, which involves a simple precipitation reaction between Mn^{2+} and $[Fe(CN)_6]^{4-}$.[45] However, this method has some drawbacks, as it can result in material defects. For instance, the rapid precipitation process can create $[Fe(CN)_6]^{4-}$ vacancies, which may lead to structural collapse during charging and discharging, and lower the diffusion rate of sodium ions, ultimately reducing the material's capacity.[46,47,49] Additionally, the presence of interstitial water in the material can cause irreversible capacity and side reactions.[46,48] Therefore, further research is needed to find a method for synthesizing stable MnPBA with high sodium content and low defects.

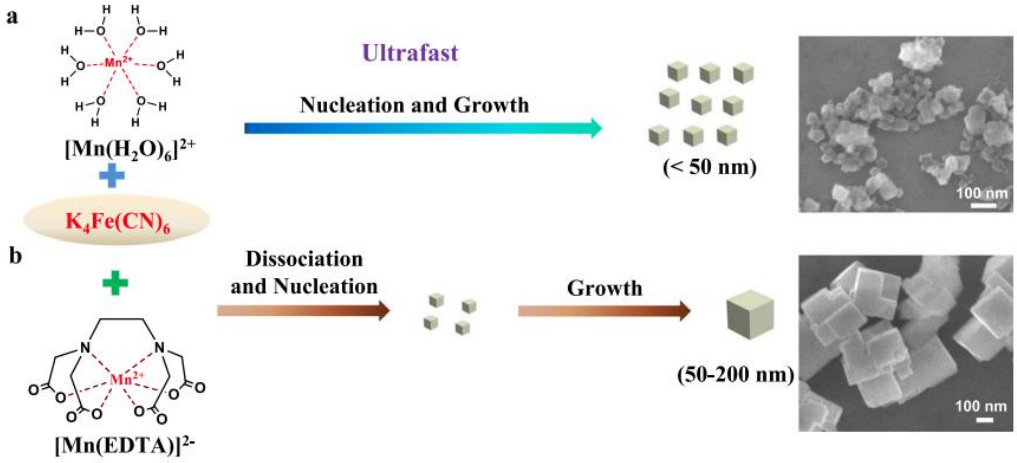

Figure 1.4 (a)The chelating-free method and (b) the chelating-assisted method cause different morphology in MnPBA[50]

In recent years, the introduction of chelating agents to slow down the nucleation rate has become the mainstream method for the synthesis of MnPBA. The role of the chelating agent in the co-precipitation method is described in Figure 1.4. Chelating agents such as sodium citrates[58] and EDTA[59] are commonly used in this process, while oxalate[51], pyrophosphoric salts[52], and sodium

carboxymethylcellulose[55] have also been reported. These agents can promote the formation of well-defined crystal structures, which improves the performance of PBAs in energy storage and electrocatalysis applications. Researchers have reported using sodium citrate to control the release rate of cobalt ions and to increase the crystallinity of MnPBA. For example, Yang's group both reported using sodium citrate to control the release rate of cobalt ions.[53] Xie et.al also use sodium citrates to increase the crystallinity of MnPBA.[54] The citrate-assisted material also exhibited larger average particle size and better initial discharge capacity (144.0 $mA{\cdot}h{\cdot}g^{-1}$ at 0.1C) than the material without chelating agents. However, the complexation ability for Mn^{2+} of citrates is much worse than that for Co^{2+} and Fe^{2+}.[56] $EDTA^{4-}$ is a better chelating agent to carry Mn^{2+} but its chelation ability is too strong. To address this issue, Zifeng Ma's group introduce ascorbic acid to dissociate the Mn^{2+} from $[MnEDTA]^{2+}$ to adjust the crystal crystal-growing.[59] This approach results in the highest initial capacity could reach 18 $mA{\cdot}h{\cdot}g^{-1}$ at 0.1C and 82% retention rate after 500 cycles.

Apart from the chelating-assisted method, there are some studies by regulating the parameters or using different techniques, to improve the performance of PBA. As one of the first reports on sodium MnPBA, Goodenough et.al slowed down the crystallization rate by increasing the sodium-ion concentration. The material reached a high capacity and cycle stability (it delivers a reversible capacity of 150 $mA{\cdot}h{\cdot}g^{-1}$ at 3.5 V in a sodium half-cell) while removing interstitial water. Ma's group researched the temperature influence on the crystallinity of materials.[60] They found that the lower temperature is beneficial to the crystallinity of material, while almost not affecting morphology.

Among these researches on sodium MnPBA, we chose the synthesis methods with and without complexing agents, respectively, and compared the obtained material properties by parameter

optimization, synthesis, and characterization. Thus, we select the best synthesis strategy and pathway and extend it to the application of potassium batteries.

1.2 Research Objectives

Broadly, the thesis will provide a detailed optimization process and characterization of NVP and Na-PBA.

Objective 1: Optimization and Characterization of Sodium Vanadium Phosphate.

The objective of this study was to optimize the synthesis procedure of NVP using the hydrothermal-assisted sol-gel method. Through the optimization of annealing temperature, as well as the addition sequence and content of ascorbic acid, we were able to identify the key phenomenon that determines the performance of the material.

Objective 2: Optimization and Characterization of Sodium Prussian Blue Analog.

This study aimed to optimize the synthesis procedure of Na-PBA. To achieve this, we synthesized the materials using both chelating-assisted and chelating-free methods, while optimizing various conditions such as ethanol content, aging time, washing solvent, and the injection of ascorbic acid. The synthesized materials were then evaluated for their performance using the sodium coin half-cell. Through this process, we identified the optimal conditions for synthesizing sodium PBA, which produced the best results.

1.3 Thesis Outline

This thesis will provide a comprehensive account of the optimization process for the synthesis of sodium-ion cathode material, along with the characterization results. The thesis will consist of three chapters that outline the tasks undertaken to achieve the research objectives. In **Chapter 2**, the optimization of NVP will be discussed, while **Chapter 3** will present two methods for synthesizing Na-PBA, along with their optimization processes and characterization. Finally, **Chapter 4** will offer concluding remarks and highlight future research directions.

Chapter 2: NVP Synthesis

2.1 Experimental Method

2.1.1 Synthesis

Materials: vanadium oxide (V_2O_5, ≥99.6%), ammonium phosphate monobasic ($NH_4H_2PO_4$, anhydrous, ≥98%), sodium carbonate (Na_2CO_3, anhydrous, ≥99.5%), L-ascorbic acid (anhydrous, ≥99%), poly (ethylene glycol) (PEG-400). Sodium hexafluorophosphate (NaPF6, >99%, Alfa Aesar), Polypropylene-Polyethylene-Polypropylene (PP-PE-PP) tri-layer battery separator (tri-layer PE, Celgard 2325, 25 μm thickness)

Method: The nanocomposite NVP@C is obtained by hydrothermal assisted sol-gel method. In this method, add 4mmol V_2O_5 to 17.5mL of deionized water, then sonicate for 20 minutes to disperse the particles evenly in the water. Then dissolve 12mmol $NH_4H_2PO_4$, and 6mmol Na_2CO_3 separately in 17.5mL deionized water (DI water) and slowly drop the solutions to V_2O_5 in order. Keep stirring magnetically at room temperature in the beaker. Then 6mL polyethylene glycol 400 (PEG-400) would be added. Finally, dissolve 6mmol ascorbic acid in 17.5mL DI water and add the solution dropwise subsequently. The whole process was completed at room temperature and exposed to an air atmosphere. Keep stirring for 30 min, the formed blue suspension was transferred to a 100mL Teflon-lined autoclave and then sealed at 180°C for 40h. Afterward, the autoclave is normally cooled to room temperature. The obtained brown mixture was treated by ultrasonic for 90min to disperse evenly and then heated by a water bath at 95°C to condense the solution The resulting material was dried at 120°C for 24h. This precursor was fully grounded and preheated at 350°C for 4h The preheated material was

also completely grounded and annealed at 750°C for 6 hours. Both preheating and annealing processes were carried out in a tube furnace and argon atmosphere.

2.1.2 Characterization Method

The powder X-ray diffraction (XRD) data collect from Rigaku D-Max-B Powder Diffractometer with Cu Kα radiation (λ = 1.5416 Å). Morphological images of the samples were recorded by scanning electron microscope (SEM) from Thermofisher Quattro S environmental scanning electron microscope.

2.1.3 Electrochemical Measurements

The coin cells used for electrochemical measurements were assembled inside an argon-filled glovebox. The cathode, made of NVP@C, was created by applying a slurry containing NVP, carbon black, and Polyvinylidene fluoride (PVDF) (in a weight ratio of 8:1:1) onto an 8mm diameter piece of Al foil and cutting it to size. The anode consisted of a 10mm diameter copper foil aiming to make an anode-free battery. The working electrodes were dried overnight at 120°C and had a loading mass of 1-2mg of NVP@C each.

The anode-free coin cells were fabricated in a glovebox with oxygen- and moisture-level less than 0.01ppm. The electrolyte used in the cells was 1M $NaPF_6$ dissolved in diglyme. The separator employed was a tri-layer polyethylene. The voltage range constricts from 0.5V to 3.8 V. The Land battery testing system was utilized to conduct galvanostatic charge and discharge experiments at room temperature and the capacity is obtained from the test result. The specific capacities and efficiency of the batteries were computed using the LAND system, and the formula is shown below:

$$ScapD = \frac{C_D}{(m-2.3)\cdot wt\%\cdot 10^{-3}} \qquad (1.1)$$

$$Efficiency = \frac{C_D}{C_C} \qquad (1.2)$$

ScapD is the specific discharging capacity; C_D is discharging capacity; C_C is the charging capacity; *m* is the mass of cathode material; *wt%* is the mass ratio of active material.

2.2 Results

2.2.1 Initial Experiment

In the initial experiment, the powder of V_2O_5, $NH_4H_2PO_4$, and Na_2CO_3 was added together at the same time. Other procedures have followed the method mentioned above.

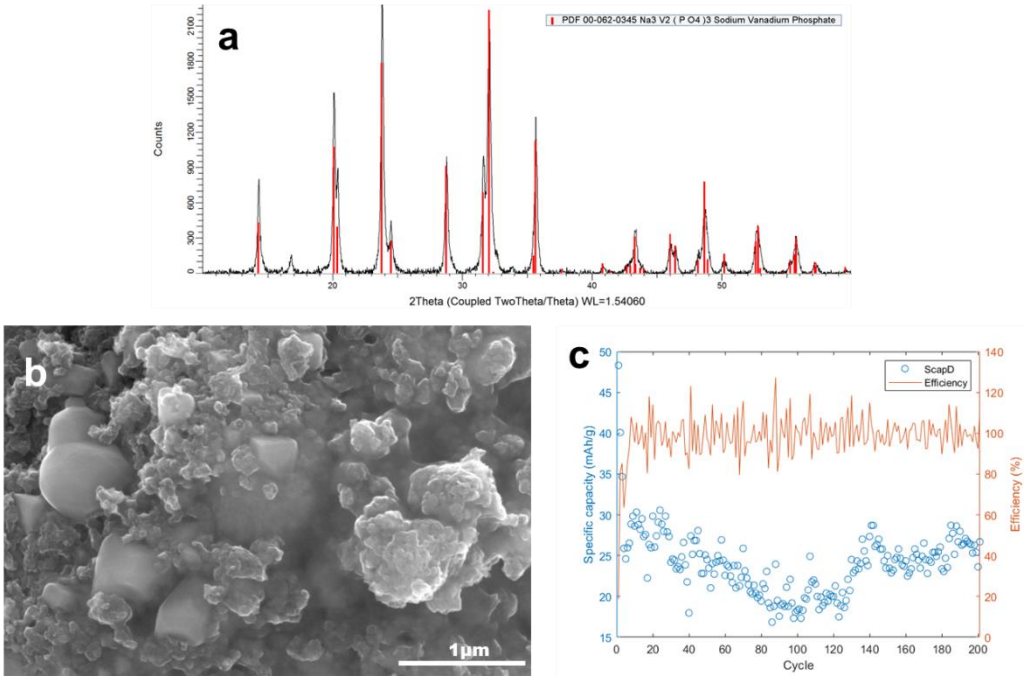

Figure 2.1 (a)XRD pattern of the initial product compared with standard PDF card; (b) SEM image of the prepared samples; (c) Capacity retention of NVP initial product

The X-ray diffraction (XRD) pattern depicted in Figure 2.1(a) confirms the successful synthesis of NVP, although the intensity of the pattern is low and there is still an impurity peak present. The scanning electron microscopy (SEM) image in Figure 2.1(b) reveals that the resulting material suffers from significant agglomeration. Furthermore, the Cycle-Efficiency & Capacity plot in Figure 2.1(c) demonstrates fluctuating efficiency, with the maximum capacity of the batteries reaching only 38.80mAh/g, which is much lower than the theoretical capacity of NVP (118mAh/g). Based on these findings, it is hypothesized that reactive molecules present in the air during the high-temperature synthesis process, due to the lack of preheating and annealing in a strict argon environment, may have reacted with the material and caused the formation of impurities. Additionally, the issue of obtaining uniformly sized nanoparticles of the material is another challenge that needs to be addressed.

2.2.2 Annealing pressure conditions

Previous studies in other materials have proposed annealing at high temperatures and pressure to obtain more uniform and dense crystals.[61,62] This approach served as the basis for optimizing NVP in our study. To achieve this, we create a critical vacuum in the tube furnace, which was then refilled with argon gas to create a controlled argon atmosphere. By adjusting the amount of argon gas, we varied the pressure and evaluated the performance of each NVP synthesized under different conditions, as depicted in Figure 2.2.

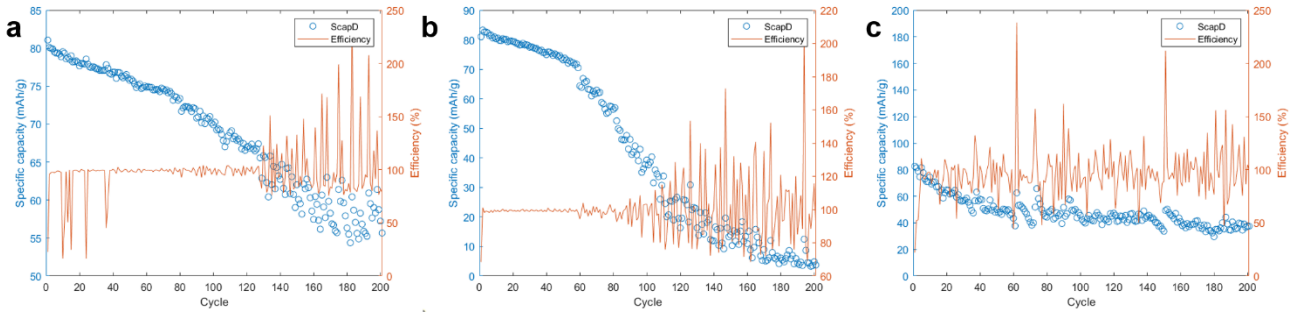

Figure 2.2 (a) Capacity retention of NVP negative-pressure product; (b) Capacity retention of NVP positive-pressure product; (c) Capacity retention of NVP regular-pressure product

In our controlled experiments, we observed that the maximum capacity achieved under negative, positive, and regular pressure was 82.15 mAh/g, 83.27 mAh/g, and 81.49 mAh/g, respectively. Despite minor variations, there was little difference in the capacities obtained under different conditions, and the retention rates were relatively low, indicating that the material was not yet stable. However, compared to the initial experiment, the capacity of these batches was significantly higher. Hence, we concluded that annealing pressure may not have a significant impact on the material's performance in a coin cell. Instead, we suspect that the strict argon atmosphere created during the annealing process may be the primary cause of capacity enhancement. In subsequent experiments, we utilized a vacuum pump to create a vacuum before refilling with argon gas to ensure a more rigorous argon gas protection atmosphere.

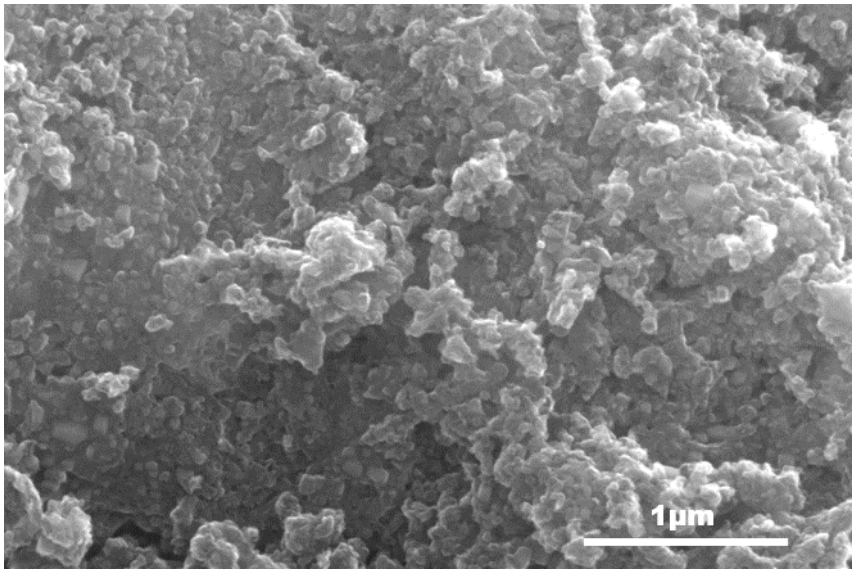

Figure 2.3 SEM images of the positive-pressure annealing NVP

Figure 2.3 displays the morphology of the material. Under positive pressure conditions, the morphology of the material does not show uniform and dispersed particles. Therefore, we believed pressure cannot impact the morphology of material. In conclusion, annealing pressure is not a fatal condition to impact the performance of NVP. We kept the regular annealing pressure and critical argon atmosphere in the following experiments.

2.2.3 Annealing temperature condition

The temperature of annealing is the crucial factor that affects the crystallinity of materials. As demonstrated in Figure A1, no peaks were observed before the annealing process, indicating that annealing was the sole mechanism responsible for generating crystallinity in the material. In a previous study conducted by Zhou[63], the optimal performance was achieved at 800°C for 8 hours of annealing. Therefore, we increased the temperature and duration of the annealing process to 800°C for 6 hours.

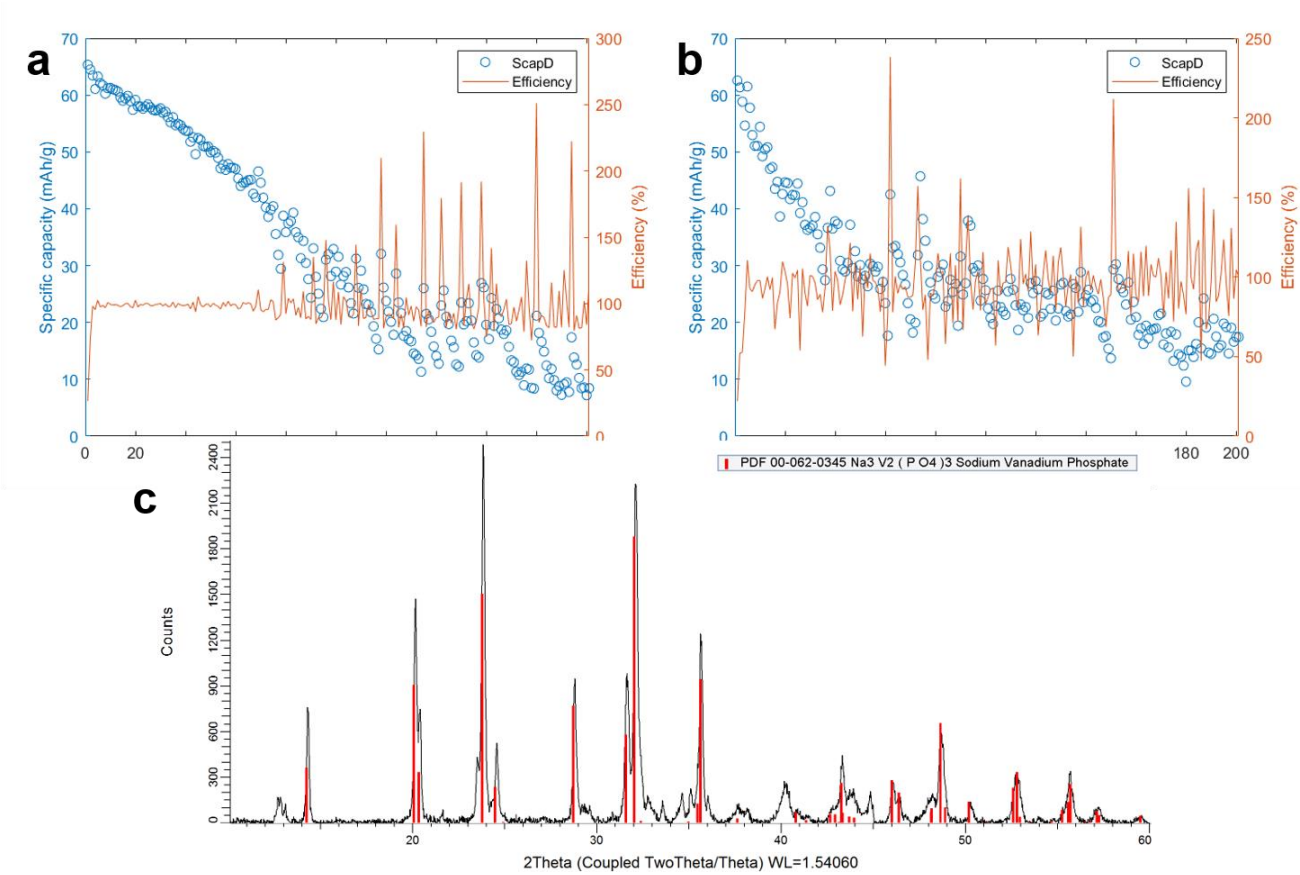

Figure 2.4 (a) Capacity retention of NVP 800°C-annealing product; (b) Capacity retention of NVP 650°C-annealing product; (c) XRD pattern of NVP 800°C-annealing product.

The performance of NVP under annealing at 800°C, as shown in Figure 2.4(a), was worse than the material annealed at the regular temperature of 750°C, with the highest capacity only reaching 65.33mAh/g. The XRD pattern exhibited many impurity peaks in Figure 2.4(c), indicating distortion in the material under higher pressure. Furthermore, we observed crystals growing on the crucibles after annealing, which did not occur after annealing at 750°C, leading to reduced intensity in the XRD. All these phenomena suggest that excessive annealing temperature and time cause material loss and degrade cell performance. As a result, we attempted to anneal NVP at a lower temperature of 600°C, but this resulted in poor performance and fluctuating efficiency. Therefore, we concluded that a lower

annealing temperature could make the material unstable. Consequently, we maintained an annealing temperature and time of 750°C and 6h, respectively, for the remainder of the experiments.

2.2.4 More ascorbic acid treatment

The color change is a crucial indicator in material synthesis. In our reaction, the system color is expected to change to navy blue upon the addition of ascorbic acid. If the color remains green, it signifies an incomplete reaction. This is because ascorbic acid is reducible, leading to a change in vanadium valence. Ascorbic acid is also utilized as one of the carbon sources for the material, hence, we increased the content of ascorbic acid appropriately to optimize the experiment.

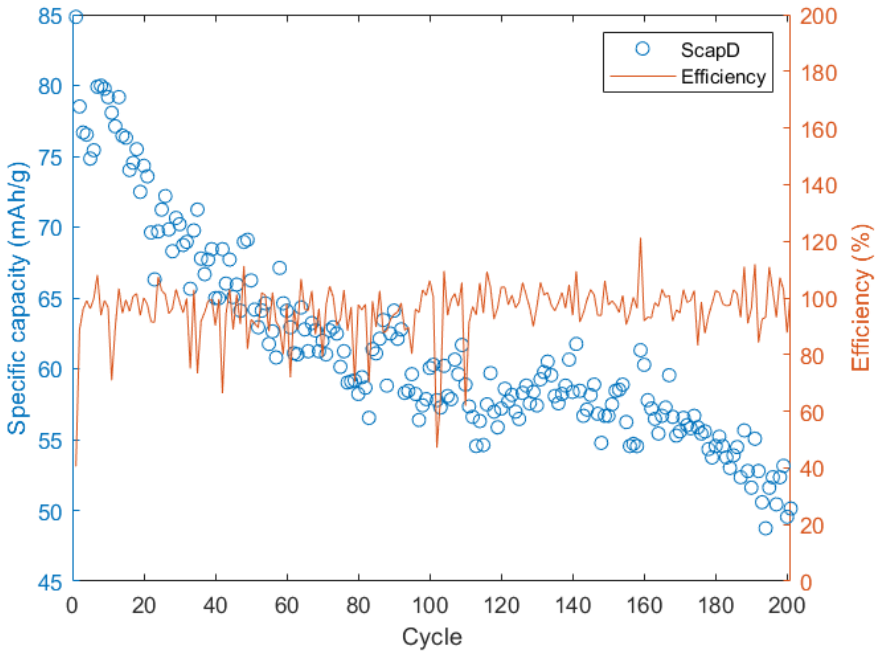

Figure 2.5 Capacity retention of NVP 8mmol ascorbic acid product

Compared with the initial experiment, we increased the amount of ascorbic acid by 2mmol and the results show in Figure 2.5. The highest capacity could reach 84.83mAh/g, which is slightly higher than previous experiments but the stability was bad. Therefore, we maintain the initial ascorbic acid amount.

2.2.5 Material addition orders and pretreatments

In the previous synthesis, small and uniform NVP@C particle still wasn't formed, which could be the main reason that rendered the bad performance of batteries. According to Chen's research[27], under the combined action of ascorbic acid and PEG-400, the content of large size and amorphous NVP@C will be greatly reduced in the reaction process. The role of ascorbic acid is not only to reduce V(V) to V(III) but also to carbonize and coat NVP in advance, limiting its size growth. To get a uniform and fully reacted product, we pretreated all the reactants dissolve in the DI water and sonicate for 20min to make sure the chemicals are fully dissolved or dispersed.

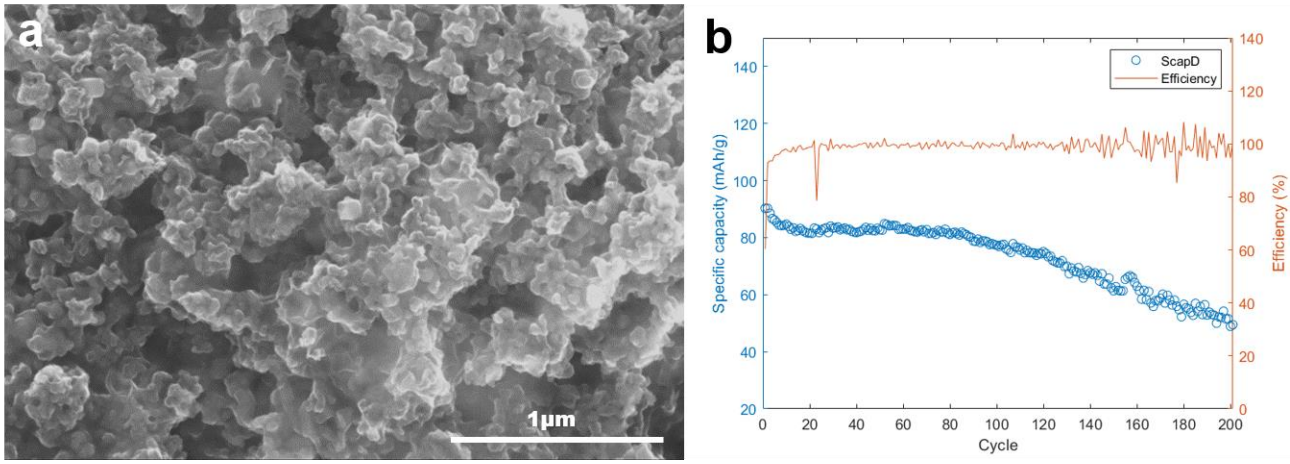

Figure 2.6 (a) SEM image of pretreatment NVP; (b) Capacity retention of pretreatment NVP

In the SEM (Figure 2.6(a)) we can see that although there is still obvious agglomeration between the particles, compared to the previous image, the particles are prominent in this image. The highest capacity from Figure 2.6 (b) could reach 92.02 mAh/g and the retention rate reaches 55.6% from the 1st cycle to the 200th cycle. This is the big progress of our experiment. During the synthesis procedure,

we found a key phenomenon which is whether the material can be dried thoroughly and which determines the success or failure of the experiment.

Figure 2.7 The appearance of the material after drying

The material, possibly due to the thick consistency of PEG-400, has been difficult to dry and typically forms a black slurry when ground. However, it should appear as depicted in Figure 2.7 and become powdery upon grinding. To assess its performance, it was hypothesized that complete drying of the material is crucial. Consequently, 5mL of ethanol was added after condensing the material to facilitate complete evaporation of the water. The results of the experiment are presented in Figure 2.8.

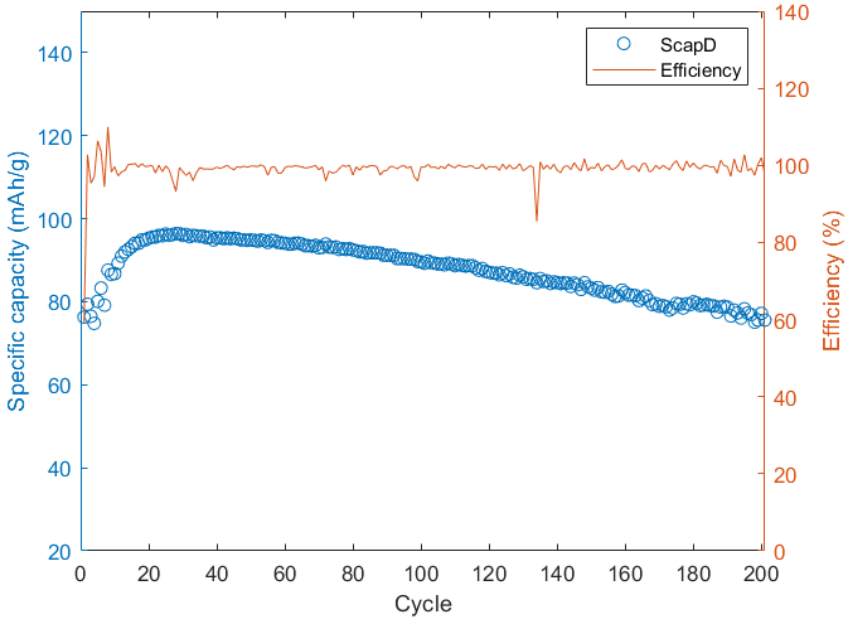

Figure 2.8 Capacity retention of ethanol-treated NVP

Adding alcohol to the material has been found to ensure its thorough drying, while also enhancing its battery performance significantly. The material exhibits a maximum capacity of 96mAh/g and delivers consistent efficiency output over time, with its capacity reaching a peak at the 20th cycle. The activation of the material during the initial electrochemical cycles is believed to be responsible for this trend.

Upon analyzing the electrochemical test results of various materials, we discovered that those with inferior performance exhibited significant fluctuations in their charging and discharging efficiency. As depicted in Figures 2.2(b) and 2.4(b), the efficiency of these materials oscillated between 50% to 200%, which was because the quality of the synthesized materials was not good enough and their capacity was also far from the theoretical capacity. Conversely, the materials that displayed superior performance (Figure 2.8) did not demonstrate such fluctuations, and in that batch, the material is

completely dried before preheating. Thus, we deduced that the dryness of the material significantly impacted material performance.

2.3 Conclusion

We conducted a study on the synthesis of NVP using a hydrothermal sol-gel assisted method, where we investigated the impact of various parameters such as annealing temperature, time, pressure, material addition sequence, and the content of ascorbic acid. Through our research, we found that the degree of drying of the material is the key to the ability of this method to produce a good-performance material. Our synthesized materials demonstrated a maximum capacity of 96mAh/g at 1C and maintained a stable output. The results of our research can provide the necessary basis for subsequent researchers using the hydrothermal sol-gel assisted method to synthesize NVP and to test the experimental results.

Chapter 3: PBA Synthesis

3.1 Experimental Method

3.1.1 Synthesis

Sodium PBA was synthesized by the co-precipitation method.

Materials: manganese (II) chloride tetrahydrate ($MnCl_2 \cdot 4H_2O$, ≥99%); sodium hexacyanoferrate (II) decahydrate ($Na_4Fe(CN)_6 \cdot 10H_2O$, ≥99%); sodium chloride (NaCl, ≥99%); Ethylenediaminetetraacetic acid tetrasodium salt hydrate ($Na_4EDTA \cdot xH_2O$, 99.0%); L-Ascorbic acid (anhydrous, ≥99%)

Chelating-free Method: This method does not involve the use of a chelating agent to induce precipitation. To make Solution A, 6 mmol of $MnCl_2 \cdot 4H_2O$ was dissolved in a 100 mL ethanol and water mixture (EtOH: H_2O=1:3) and degas the solution for 15min. Solution B consisted of a 100 mL solution containing 3 mmol $Na_4Fe(CN)_6$ and 14g NaCl. Note that $Na_4Fe(CN)_6$ is first completely dissolved in DI water before adding ethanol and NaCl. Solution B is added dropwise to Solution A at a rate of 1 mL/min while vigorously stirring, and the resulting mixture is aged for either (1) 3 hours, (2) 6 hours, or (3) 12 hours to allow for comparison. All the synthesis procedures were under N_2 protection. The white precipitate is then separated by centrifugation and washed with DI water or the ethanol and water mixture three times. Finally, the material is dried at 100°C under vacuum for 24 hours.

Chelate-assisted Method: We followed the synthesis method outlined in the research papers by Zifeng Ma et al.[59] and Yujie Zhu[18] et al. with some minor adjustments. Firstly, we mixed 6 mmol of $MnCl_2$ and Na_4EDTA in 60 mL of DI water with vigorous stirring until completely dissolved. Next, the solution was slowly added dropwise at a 1 mL/min rate into a separate solution of 60 mL of $Na_4Fe(CN)_6$. Afterward, 0.2 M ascorbic acid was injected into the same solution at a rate of 0.5 mL/min. The solution was stirred for 1 hour at room temperature, then aged for 6 hours. The resulting material was then centrifuged and washed three times with DI water. Finally, the material was dried under a vacuum at 100°C overnight.

3.1.2 Schlenk Line setup

The Schlenk line is a system with a dual manifold comprising a vacuum manifold that connects to a vacuum pump and a gas manifold that connects to a nitrogen cylinder. As illustrated in Figure 3.1(a), the Schlenk line consists of four ports equipped with rubber tubes and needles for degassing and creating a nitrogen atmosphere for reactions. The double oblique taps connect the two manifolds and are utilized for controlling nitrogen filling and vacuuming. Figure 3.1 (b) demonstrates how the tap can be adjusted to accommodate various conditions.

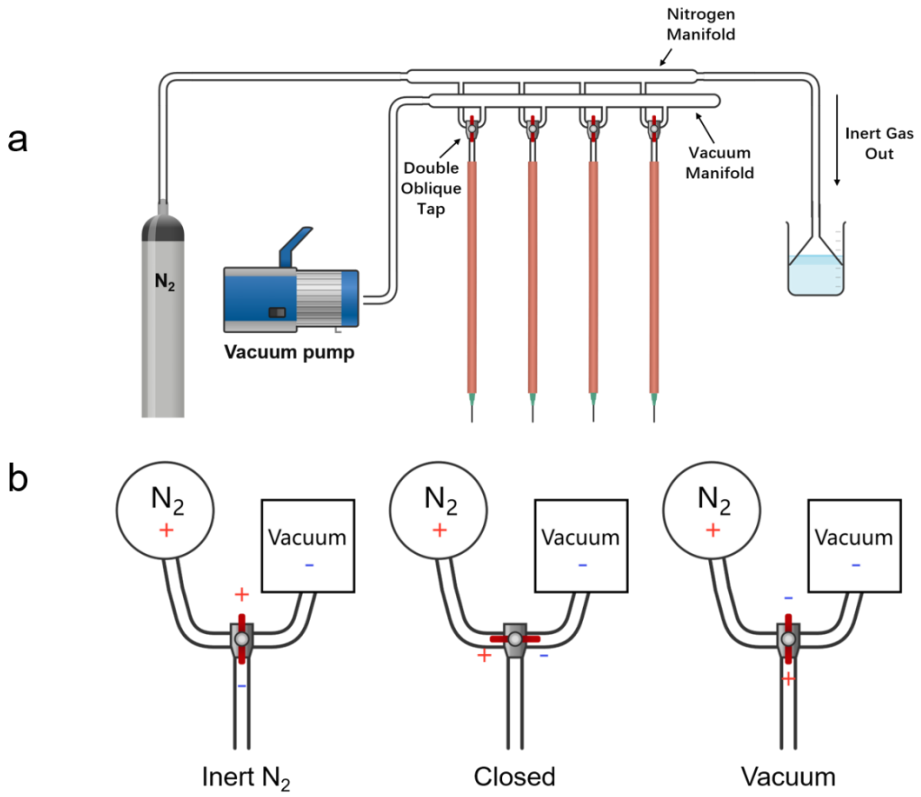

Figure 3.1 (a) Schematic diagram of the Schlenk line; (b) Schematic diagram of vacuum and nitrogen protection systems by valve changeover

3.1.3 Characterization Method

The X-ray diffraction (XRD) images were obtained using a Rigaku D-Max-B Powder Diffractometer equipped with Cu Kα radiation (λ = 1.5416 Å). Morphological characterization was carried out using a Thermofisher Quattro S environmental scanning electron microscope. Thermogravimetric analysis (TGA) was performed using a Q 5000 IR instrument (TA Instruments) under a nitrogen atmosphere with a heating rate of 10 ˚C min^{-1}. Data for element mapping was obtained using an Oxford AzTec Energy Dispersive X-ray Spectrometer (EDXS).

3.1.4 Electrochemical measurements

The working electrode (cathode) included the active materials, PVDF binder, and carbon black with a ratio of 7:2:1. The electrode slurry was evenly applied to the aluminum foil and cut into 8mm diameter round pieces. Each piece of electrode contained 0.7-1.2mg active material. The electrode foil was dried under a vacuum at 100°C overnight.

The electrochemical measurements were conducted using coin half-cells made of sodium and potassium. The electrolyte used was a mixture of 1M $NaClO_4$ in 1:1 dimethyl carbonate/ethylene carbonate electrolyte (DMC/EC) with 10 wt. % fluoroethylene carbonate (FEC). Glass fiber was used as the separator, while metallic sodium was used as the counter electrodes. Galvanostatic charge-discharge tests were carried out at room temperature using a Land battery test system within the voltage range of 2.0-4.0V versus Na/Na^+. The efficiency and the specific capacities are calculated by the LAND system, and the calculation follows the formulas 1.1 and 1.2 mentioned above.

3.2 Results

3.2.1 Chelation-free method

The ethanol content in solvent: The performance of PB can be significantly affected by the presence of interstitial water. This is because the side reactions of interstitial water during charging and discharging can cause deformation and irreversible capacity loss of the material. However, since the co-precipitation method used to synthesize PBA is inevitably performed in water, it is necessary to find ways to reduce the water content in the solution during synthesis to minimize its negative impact on the material. One possible solution is to use an organic agent to reduce the water content in the

solution. Ethanol is an ideal solvent in this regard, as it is miscible with water in any ratio. By using ethanol to reduce the amount of water in the reaction mixture, we can minimize the side reactions caused by crystalline water and improve the performance of PBA. To test the effectiveness of using ethanol as a solvent for PBA synthesis, we conducted three experiments using different water and alcohol ratios in the reaction mixture. In the first experiment, we used only water as the solvent, and named the product PBA_W, while in the second and third experiments, we used water and alcohol ratios of 3:1 and 9:1, and named these two products as PBA_E9 and PBA_E3, respectively. The results of these experiments are shown in Figure 3.2.

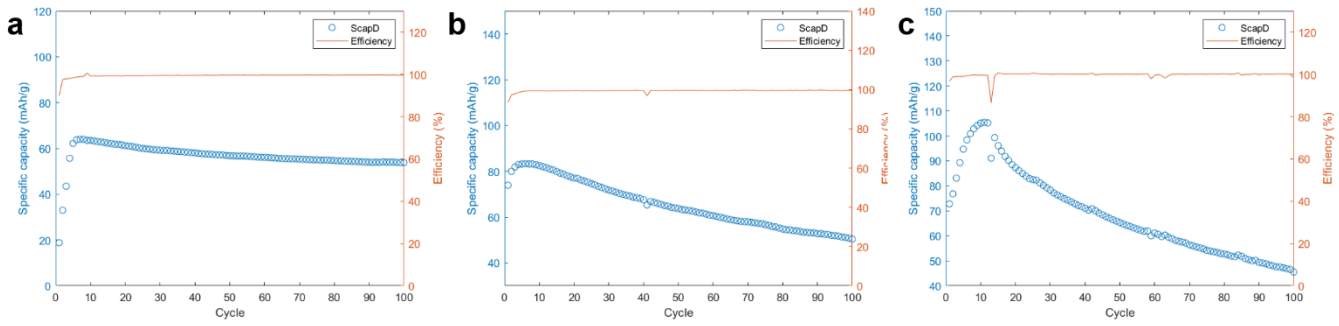

Figure 3.2 (a)Capacity retention of PBA_W; (b) Capacity retention of PBA_E9; (c) Capacity retention of PBA_E3

As can be seen from the figure, the use of ethanol as a solvent for PBA synthesis resulted in significantly improved performance of the material. The highest initial capacity for PBA_W, PBA_E9 and PBA_E3 are 64.0mAh/g, 83.3mAh/g, and 105.4mAh/g. In particular, the PBA synthesized using a water and alcohol ratio of 3:1 showed the best performance, with a higher capacity and better cycling stability compared to the other two samples.

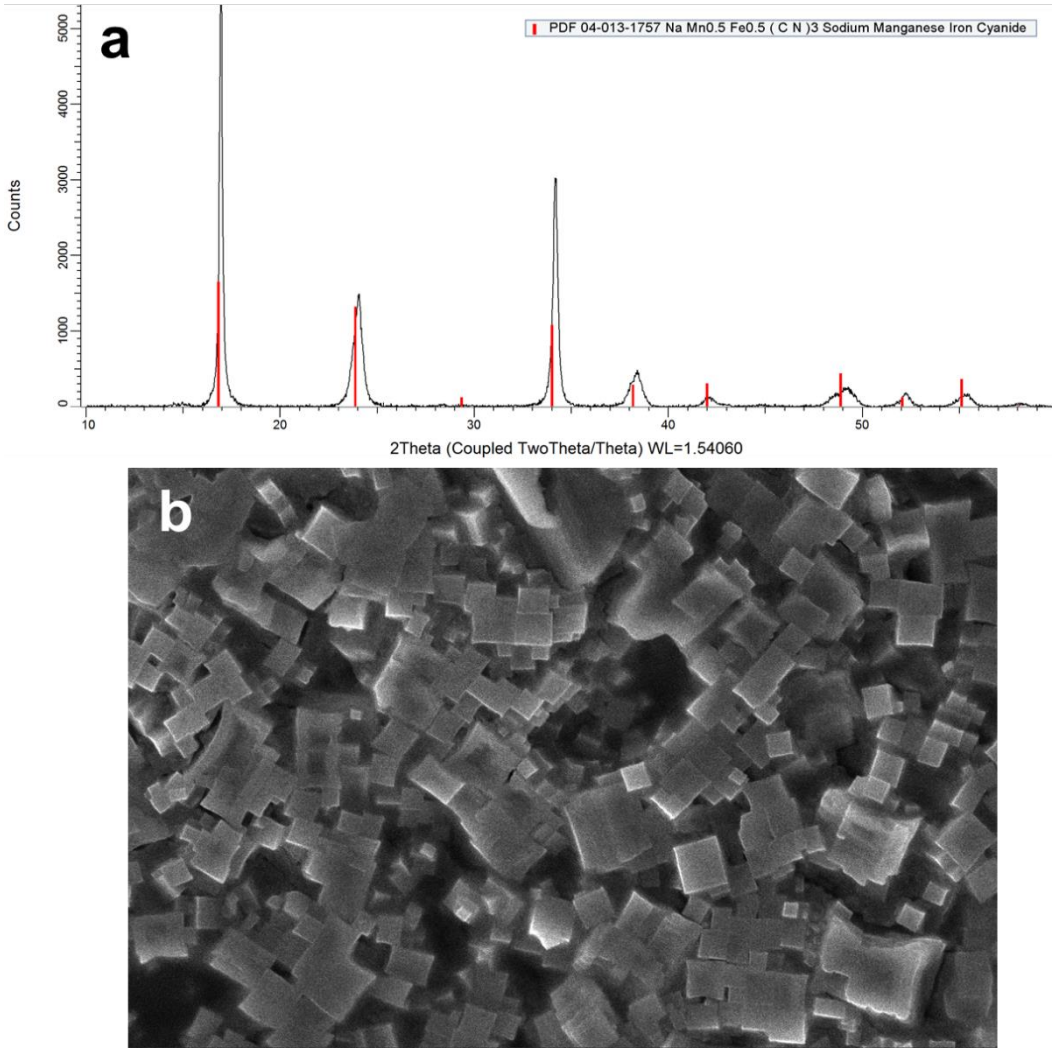

Figure 3.3 (a) XRD pattern of PBA_E3; (b) SEM image of PBA_E3

Figure 3.3(a) displays the XRD pattern of PBA_E9, which shows the characteristic peaks of the rhombohedral structure of PBA. This indicates that the presence of ethanol in the reaction mixture did not affect the generation of PBA precipitation and the resulting PBA retains its desired structure. However, the SEM image shown in Figure 3.3(b) reveals that the PBA particles have a large size of 400nm and also exhibit some degree of agglomeration. This may be due to the slower precipitation rate of PBA in the presence of ethanol, leading to larger particle size and agglomeration. In summary, using ethanol to reduce the water content in the reaction mixture is a good strategy to minimize the

negative impact of interstitial water on the performance of PBA. And 1:3 is the best ratio of ethanol and water for the reaction.

Washing agent: In order to minimize the amount of interstitial water present in PBA, a 1:3 solution of ethanol and water was used to wash the material during centrifugation instead of deionized water. This is because we assumed the use of organic solvents like alcohol can help to reduce the amount of water present in the PBA structure, which can have a positive impact on its performance.

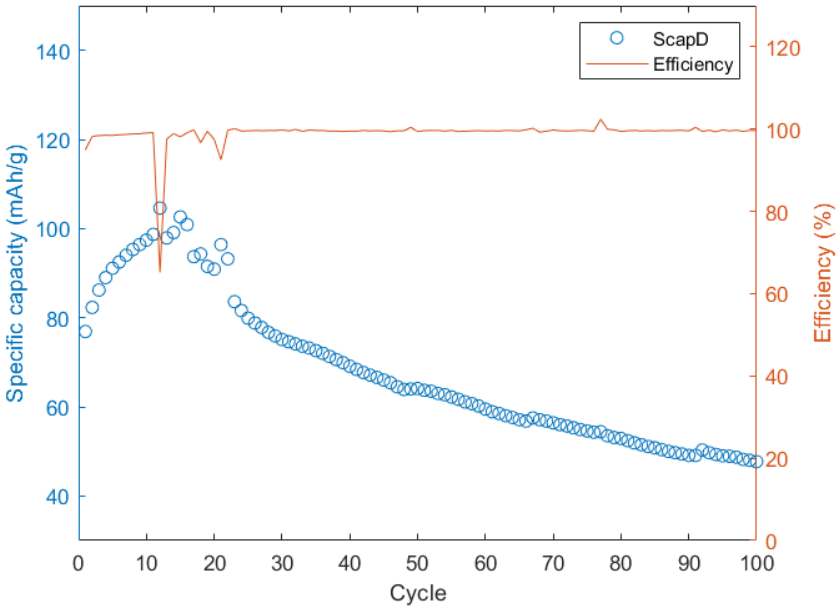

Figure 3.4 Capacity retention of ethanol solution washed PBA

In terms of material performance, we observed that the use of the 1:3 alcohol-water solution for washing PBA led to a specific capacity of up to 102.4mAh/g, which is comparable to the performance observed when using deionized water for washing. We also changed the aging time to 12 hours and

washed the PBA with both deionized water and the 1:3 alcohol-water solution. Here are the SEM images in Figure 3.5

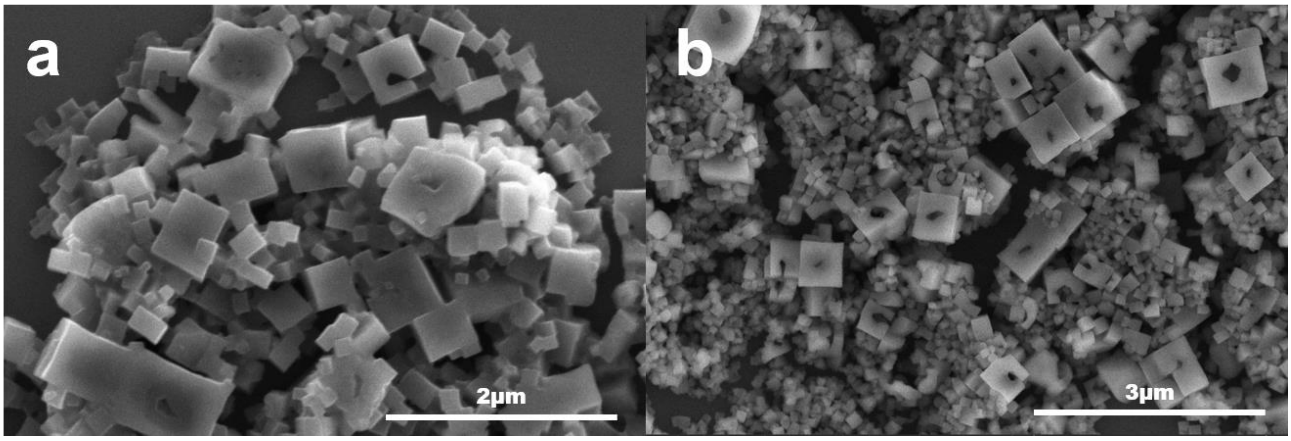

Figure 3.5 (a) XRD pattern of water-washed material; (b) SEM image of ethanol solution-washed material

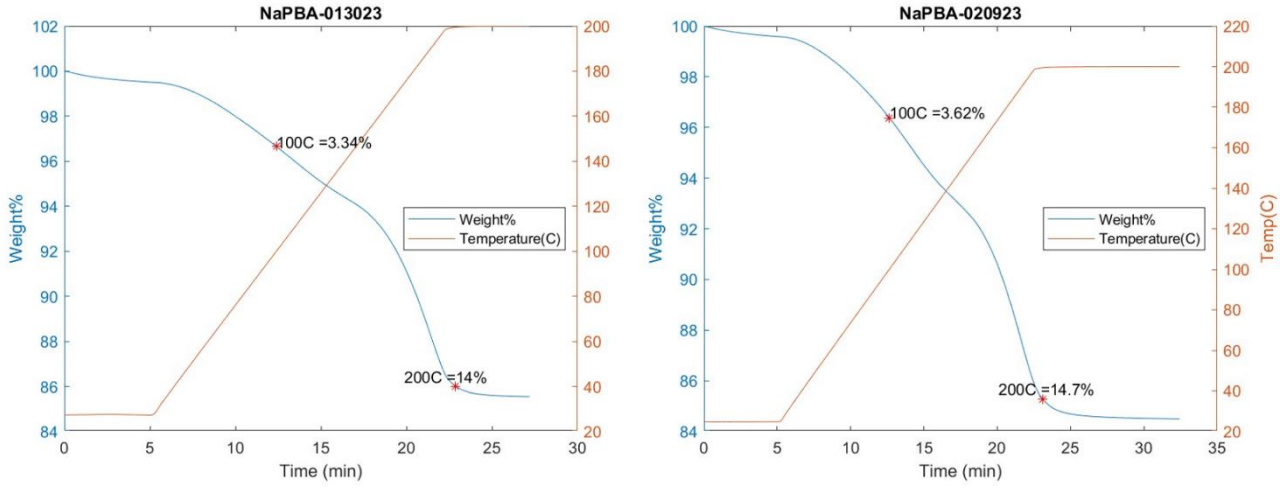

Figure 3.6 (a) TGA test result of water-washed material; (b) TGA test result of ethanol solution-washed material

By comparing the two SEM images, we observed that the PBA material washed with ethanol had more holes and small pits compared to the material washed with water. This may be due to the fact that ethanol is more volatile than water and can therefore lead to greater surface erosion of the PBA crystals during washing. In terms of interstitial water content, the TGA curves in Figure 3.6(a) show two stages

of weight loss at temperatures of 100°C and 200°C, corresponding to the loss of interstitial water and coordinated water, respectively. Interestingly, we found that the interstitial water content of the PBA material washed with the two liquids did not change much, despite the observed differences in crystal morphology. Therefore, we abandoned using ethanol solution to wash the material

Aging time: Aging time is another important factor to influence crystal growth. In particular, prolonged aging can cause interstitial water to leave the crystal, leading to a smaller crystal size. Hou et al.[64] proposed that the amount of interstitial water present in the crystal is a critical factor that affects the dissolution and recrystallization processes, and longer aging times can lead to the removal of interstitial water from the crystal lattice, resulting in a smaller crystal size. To investigate the impact of aging time on PBA properties, we conducted experiments with aging times of 3h, 6h, and 12h and named these three materials PBA_3h, PBA_6h, and PBA_12h.

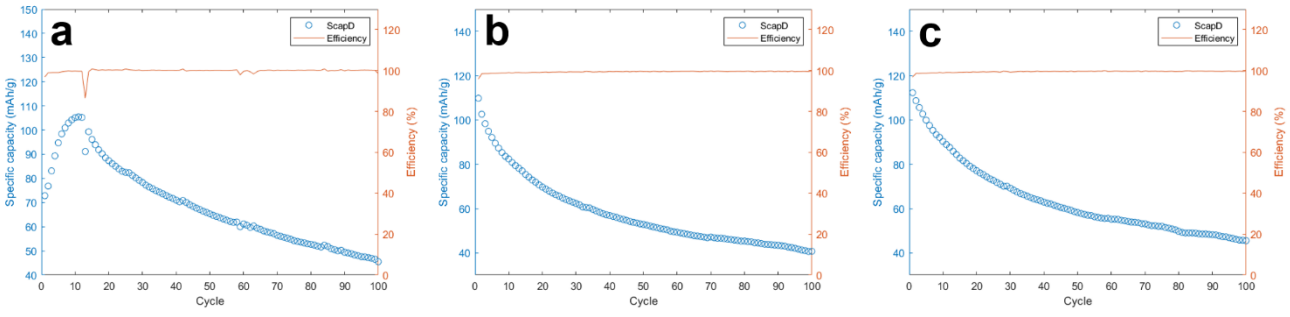

Figure 3.7 (a) Capacity retention of PBA_3h; (b) Capacity retention of PBA_6h; (a) Capacity retention of PBA_12h

In Figure 3.7, we observed that the PBA samples aged for longer periods (6h and 12h) exhibited higher initial capacity values (109.6mAh/g and 112mAh/g, respectively) compared to the sample aged for 3h (105.4mAh/g). This suggests that a longer aging time can result in a material with better capacity. However, as shown in the SEM image, longer aging times also resulted in the formation of small pits

and holes in the PBA crystals, which may be the main reason for the poor retention rate of the material. This is consistent with previous observations that longer aging times can lead to decreased cycling stability, regardless of the washing solvent used. Overall, our results suggest that while longer aging times can result in PBA materials with higher initial capacity values, they may also lead to decreased cycling stability due to the formation of small pits and holes in the crystals.

3.2.2 Chelation-assisted method

With the injection of Ascorbic Acid: In this method, we choose tetra-sodium EDTA as the chelating agent, since $EDTA^{4-}$ has strong chelating ability to Mn^{2+}. However, this also means that Mn^{2+} is hard to release from EDTA. Therefore, the ascorbic acid was introduced to release more Mn^{2+} from EDTA and reduce the defect of the product. We named the material PBA_VC

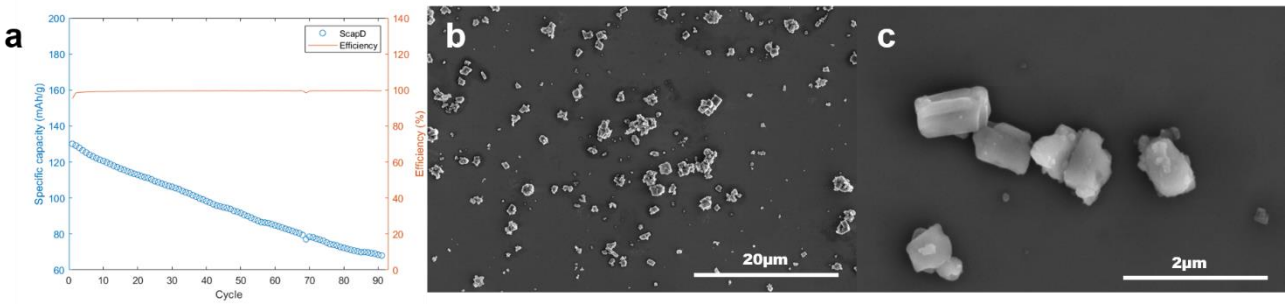

Figure 3.8 (a)Capacity retention of PBA_VC; (b) and (c) SEM images of PBA_VC;

In Figure 3.8, we can observe the SEM image of the PBA material obtained by the current method, which shows excellent dispersion and uniform particle size. The PBA particles are observed to be around 1 micron in size, with a uniform shape and size distribution. Though the crystals don't show the perfect cubic structure, the crystal morphology is not the only indicator to judge the performance

Moreover, this batch of materials has demonstrated the highest capacity we have obtained so far at 1C, reaching 130mAh/g. This is a significant improvement compared to the previous batches, which had a maximum capacity of around 112mAh/g at 1C.

Without the injection of Ascorbic acid: In order to compare with the reaction of ascorbic acid injection, we did the experiment without ascorbic acid. Figure 3.9 shows that the solution with ascorbic acid had a thicker consistency than the solution without ascorbic acid, indicating that the presence of ascorbic acid facilitated the release of more manganese cations in the solution, resulting in increased precipitation. Additionally, after centrifugation, the reaction without ascorbic acid produced less product. These findings are consistent with the conclusions drawn in Zifeng Ma's research.[59]

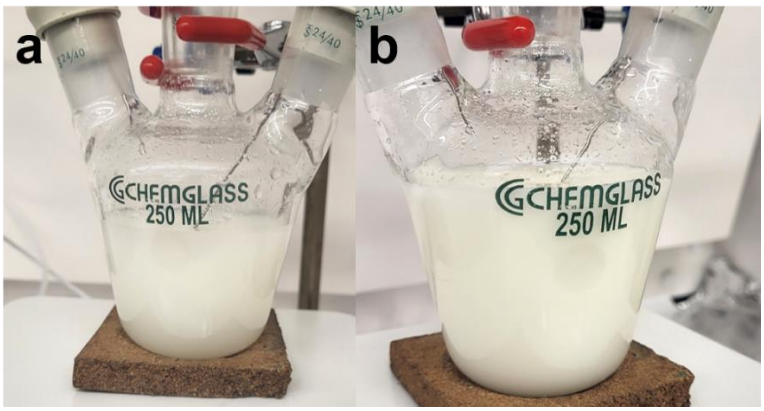

Figure 3.9 (a) the solution without ascorbic acid injection; (b) the solution with the injection of ascorbic acid.

Due to the limited yield of the reaction, we were only able to perform SEM analysis to examine the morphology of the synthesized material. As shown in Figure 3.10, the crystals exhibit an angular cubic shape. However, unlike the experiment with ascorbic acid injection, the particles, in this case, display an uneven size distribution and severe agglomeration. To further investigate the electrochemical properties of the material synthesized by this method, we plan to scale up the synthesis in the next step.

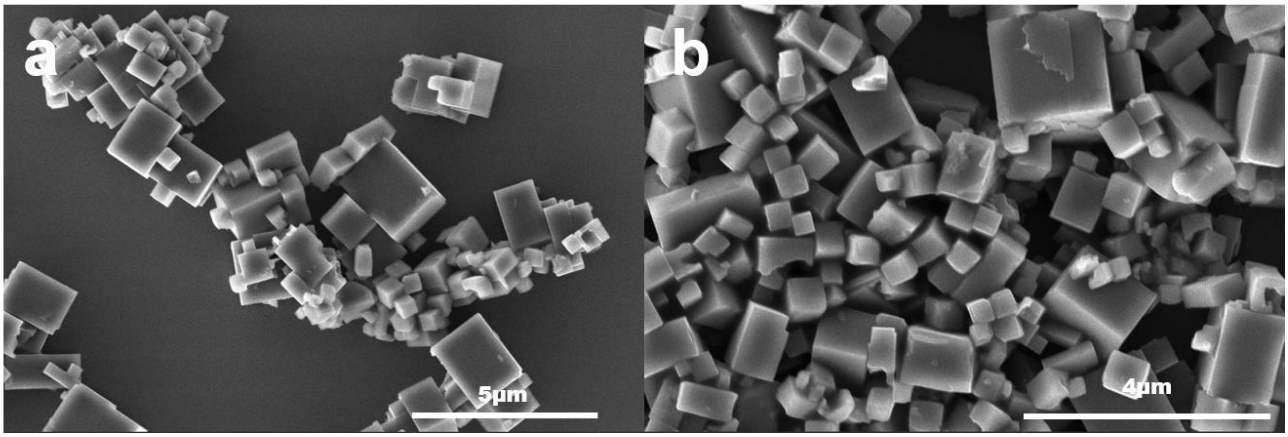

Figure 3.10 SEM images of PBA synthesis without injection of ascorbic acid

In summary, the current method for synthesizing PBA materials using tetra-sodium EDTA as a chelating agent and ascorbic acid as the dissociating agent has shown great advantages and prospects. The two reagents introduced reduced the nucleation rate of the crystals and grew uniform and well-dispersed PBA crystals, resulting in materials with higher capacity and better cycling stability. Further optimization of parameters such as aging time, aging temperature, and other aspects may lead to even better performance and improved stability of PBA materials.

3.3 Conclusion

The use of two distinct approaches in this program has allowed for a comprehensive evaluation and optimization of the Na_PBA material synthesis. The chelation-free method utilized orthogonal experiments to determine the optimal combination of parameters, resulting in a material with a specific capacity of 112mAh/g at 1C. The method uses chelating agents, specifically adding EDTA and ascorbic acid, allowing for even further enhancement of the material properties, resulting in a specific capacity of 130mAh/g at 1C.

This research has expanded and improved the synthesis of Na_PBA and provides novel insights and methodology for future studies on PBA synthesis. The use of orthogonal experiments and chelating agents can serve as valuable tools for optimizing the synthesis of other materials and can be applied to a variety of other research areas as well. Overall, this research has made significant contributions to the field of energy storage and materials science.

Chapter 4: Conclusions and Outlook

4.1 Conclusions

This thesis first demonstrated the optimization of Sodium Vanadium Phosphate. The study examined the impact of various synthesis conditions, including annealing temperature, annealing pressure, ascorbic acid content, and the order of material addition, on the resulting materials. The findings indicated that high capacity and cyclic stability were achieved when the reactants were well-dispersed at the start of the reaction and completely dried without any black slurry. This study provides a crucial synthetic index for the hydrothermal reaction synthesis of NVP.

In the second part of the thesis, we discover the Sodium Prussian Blue Analog (PBA, a promising sodium cathode material. We conducted two synthesis methods - one with a chelating agent and the other without. In the chelation-free method, we optimized the conditions of ethanol content, aging time, and washing reagents, and found that the highest capacity of 112 mAh/g at 1C was obtained with an ethanol ratio of 1:3, aging time of 12 hours, and deionized water as the washing solvent. In the method with a complexing agent, we used tetra-sodium EDTA as the chelating agent and added ascorbic acid as a dissociating agent. This method produced a material with a good dispersion system and achieved a capacity of 130 mAh/g at 1C. We plan to optimize future PBA synthesis based on this method and extend it to KPBA synthesis as much as possible.

In summary, we have successfully optimized the synthesis conditions for two sodium cathodes, NVP and PBA materials, to enhance their performance, producing exceptional materials. Our goal is to

accelerate the development and widespread adoption of high-performance sodium electrode materials by optimizing synthesis conditions and obtaining superior materials

4.2 Outlook

NVP and Na_PBA are two promising electrode materials for the new generation of sodium batteries due to their high capacity and stability. We have optimized the synthesis methods for these materials and investigated the effects of their morphology and structure on their performance. Our findings can provide ideas and inspiration for future research on these two battery materials.

Through our optimization efforts, we were able to synthesize NVP and Na_PBA with high purity and improved electrochemical properties. We also found that the morphology and structure of the materials played a critical role in their performance. For example, we observed that the size and shape of the particles, as well as the crystal structure, and the defects' presence had a significant impact on the materials' capacity, rate capability, and cycle stability.

Overall, our work provides insights into the synthesis and performance of NVP and Na_PBA, which can guide future research efforts in developing high-performance sodium battery electrode materials.

References

1. Goriparti, S., Miele, E., De Angelis, F., Di Fabrizio, E., Zaccaria, R. P., & Capiglia, C. (2014). Review on the recent progress of nanostructured anode materials for Li-ion batteries. Journal of power sources, 257, 421-443.

2. Kumar, Y., Ringenberg, J., Depuru, S. S., Devabhaktuni, V. K., Lee, J. W., Nikolaidis, E., ... & Afjeh, A. (2016). Wind energy: Trends and enabling technologies. Renewable and Sustainable Energy Reviews, 53, 209-224.

3. He, Y. L., Qiu, Y., Wang, K., Yuan, F., Wang, W. Q., Li, M. J., & Guo, J. Q. (2020). Perspective of concentrating solar power. Energy, 198, 117373.

4. Moran, E. F., Lopez, M. C., Moore, N., Müller, N., & Hyndman, D. W. (2018). Sustainable hydropower in the 21st century. Proceedings of the National Academy of Sciences, 115(47), 11891-11898.

5. Ozawa, Kazunori, ed. Lithium ion rechargeable batteries: materials, technology, and new applications. John Wiley & Sons, 2012.

6. Nayak, P. K., Yang, L., Brehm, W., & Adelhelm, P. (2018). From lithium-ion to sodium-ion batteries: advantages, challenges, and surprises. Angewandte Chemie International Edition, 57(1), 102-120.

7. Li, P., Zhao, Y., Shen, Y., & Bo, S. H. (2020). Fracture behavior in battery materials. Journal of Physics: Energy, 2(2), 022002.

8. Weiss, M., Ruess, R., Kasnatscheew, J., Levartovsky, Y., Levy, N. R., Minnmann, P., ... & Janek, J. (2021). Fast charging of lithium-ion batteries: a review of materials aspects. Advanced Energy Materials, 11(33), 2101126.
9. Shen, X., Liu, H., Cheng, X. B., Yan, C., & Huang, J. Q. (2018). Beyond lithium ion batteries: Higher energy density battery systems based on lithium metal anodes. Energy Storage Materials, 12, 161-175.

10. Hosaka, T., & Kubota, K. (2020). a. S. Hameed, S. Komaba. Research Development on K-Ion Batteries, Chem. Rev, 120, 6358-6466.

11. Dunn, Bruce, Haresh Kamath, and Jean-Marie Tarascon. "Electrical energy storage for the grid: a battery of choices." Science 334.6058 (2011): 928-935.

12. Väyrynen, A., & Salminen, J. (2012). Lithium ion battery production. The Journal of Chemical Thermodynamics, 46, 80-85.

13. Thielmann, A., Sauer, A., & Wietschel, M. (2015). Fraunhofer-Institute ISI.

14. Peters, J. F., & Weil, M. (2016). A critical assessment of the resource depletion potential of current and future lithium-ion batteries. Resources, 5(4), 46.

15. Ellis, B. L., & Nazar, L. F. (2012). Sodium and sodium-ion energy storage batteries. Current Opinion in Solid State and Materials Science, 16(4), 168-177.

16. Zhou, A., Cheng, W., Wang, W., Zhao, Q., Xie, J., Zhang, W., ... & Li, J. (2021). Hexacyanoferrate-type Prussian blue analogs: principles and advances toward high-performance sodium and potassium ion batteries. Advanced Energy Materials, 11(2), 2000943.

17. Kim, S. W., Seo, D. H., Ma, X., Ceder, G., & Kang, K. (2012). Electrode materials for rechargeable sodium-ion batteries: potential alternatives to current lithium-ion batteries. Advanced Energy Materials, 2(7), 710-721.

18. Deng, L., Qu, J., Niu, X., Liu, J., Zhang, J., Hong, Y., ... & Zhu, Y. (2021). Defect-free potassium manganese hexacyanoferrate cathode material for high-performance potassium-ion batteries. Nature communications, 12(1), 2167.

19. Okoshi, M., Yamada, Y., Yamada, A., & Nakai, H. (2013). Theoretical analysis on de-solvation of lithium, sodium, and magnesium cations to organic electrolyte solvents. Journal of the Electrochemical Society, 160(11), A2160.

20. Chayambuka, K., Mulder, G., Danilov, D. L., & Notten, P. H. (2018). Sodium-ion battery materials and electrochemical properties reviewed. Advanced Energy Materials, 8(16), 1800079.

21. Zhang, X., Rui, X., Chen, D., Tan, H., Yang, D., Huang, S., & Yu, Y. (2019). Na 3 V 2 (PO 4) 3: an advanced cathode for sodium-ion batteries. Nanoscale, 11(6), 2556-2576.

22. Zhu, Y., Xu, H., Ma, J., Chen, P., & Chen, Y. (2022). The recent advances of NASICON-Na3V2 (PO4) 3 cathode materials for sodium-ion batteries. Journal of Solid State Chemistry, 123669.

23. Klee, R., Aragón, M. J., Lavela, P., Alcantara, R., & Tirado, J. L. (2016). Na3V2 (PO4) 3/C nanorods with improved electrode–electrolyte interface as cathode material for sodium-ion batteries. ACS Applied Materials & Interfaces, 8(35), 23151-23159.

24. He, Z., Jiang, Y., Zhu, J., Wang, H., Li, Y., Zhou, H., ... & Wang, L. (2018). N-doped carbon coated LiTi2 (PO4) 3 as superior anode using PANi as carbon and nitrogen bi-sources for aqueous lithium ion battery. Electrochimica Acta, 279, 279-288.

25. Xu, X., Xiong, F., Meng, J., Wang, X., Niu, C., An, Q., & Mai, L. (2020). Vanadium-based nanomaterials: a promising family for emerging metal-ion batteries. Advanced Functional Materials, 30(10), 1904398.

26. Jung, Y. H., Lim, C. H., & Kim, D. K. (2013). Graphene-supported Na 3 V 2 (PO 4) 3 as a high rate cathode material for sodium-ion batteries. Journal of Materials Chemistry A, 1(37), 11350-11354.

27. Duan, W., Zhu, Z., Li, H., Hu, Z., Zhang, K., Cheng, F., & Chen, J. (2014). Na 3 V 2 (PO 4) 3@ C core–shell nanocomposites for rechargeable sodium-ion batteries. Journal of Materials Chemistry A, 2(23), 8668-8675.

28. Gong, Z., & Yang, Y. (2011). Recent advances in the research of polyanion-type cathode materials for Li-ion batteries. Energy & Environmental Science, 4(9), 3223-3242.

29. Fang, Y., Xiao, L., Ai, X., Cao, Y., & Yang, H. (2015). Hierarchical carbon framework wrapped Na3V2 (PO4) 3 as a superior high-rate and extended lifespan cathode for sodium-ion batteries. Advanced materials, 27(39), 5895-5900.

30. Zhu, X., Fang, Y., Ai, X., Yang, H., & Cao, Y. (2015). Na3V2 (PO4) 3/C nanocomposite synthesized via pre-reduction process as high-performance cathode material for sodium-ion batteries. Journal of Alloys and Compounds, 646, 170-174.

31. Inoishi, A., Yoshioka, Y., Zhao, L., Kitajou, A., & Okada, S. (2017). Improvement in the energy density of Na3V2 (PO4) 3 by Mg substitution. ChemElectroChem, 4(11), 2755-2759.

32. Ou, J., Yang, L., & Zhang, Z. (2019). Chrysanthemum derived hierarchically porous nitrogen-doped carbon as high performance anode material for Lithium/Sodium ion batteries. Powder Technology, 344, 89-95.

33. Zhu, Y., Xu, H., Ma, J., Chen, P., & Chen, Y. (2022). The recent advances of NASICON-Na3V2 (PO4) 3 cathode materials for sodium-ion batteries. Journal of Solid State Chemistry, 123669.

34. Huang, H. B., Luo, S. H., Liu, C. L., Yang, Y., Zhai, Y. C., Chang, L. J., & Li, M. Q. (2019). Double-carbon coated Na3V2 (PO4) 3 as a superior cathode material for Na-ion batteries. Applied Surface Science, 487, 1159-1166.

35. Jiang, S., & Wang, Y. (2019). Phosphorus-doped graphene-improved Na3V2 (PO4) 3@ C nanocomposite possessing high-rate performance for electrochemical energy storage. Ceramics International, 45(9), 11600-11606.
36. Lim, S. J., Han, D. W., Nam, D. H., Hong, K. S., Eom, J. Y., Ryu, W. H., & Kwon, H. S. (2014). Structural enhancement of Na 3 V 2 (PO 4) 3/C composite cathode materials by pillar ion doping for high power and long cycle life sodium-ion batteries. *Journal of Materials Chemistry A*, *2*(46), 19623-19632.

37. Li, Y., Chen, M., Liu, B., Zhang, Y., Liang, X., & Xia, X. (2020). Heteroatom doping: an effective way to boost sodium ion storage. *Advanced Energy Materials*, *10*(27), 2000927.

38. Wu, X., Wu, C., Wei, C., Hu, L., Qian, J., Cao, Y., ... & Yang, H. (2016). Highly crystallized Na2CoFe (CN) 6 with suppressed lattice defects as superior cathode material for sodium-ion batteries. ACS applied materials & interfaces, 8(8), 5393-5399.

39. Wang, P., Li, Y., Zhu, D., Gong, F., Fang, S., Zhang, Y., & Sun, S. (2022). Treatment dependent sodium-rich Prussian blue as a cathode material for sodium-ion batteries. Dalton Transactions, 51(25), 9622-9626.

40. Mao, Y., Chen, Y., Qin, J., Shi, C., Liu, E., & Zhao, N. (2019). Capacitance controlled, hierarchical porous 3D ultra-thin carbon networks reinforced prussian blue for high performance Na-ion battery cathode. Nano Energy, 58, 192-201.

41. Usiskin, R., Lu, Y., Popovic, J., Law, M., Balaya, P., Hu, Y. S., & Maier, J. (2021). Fundamentals, status and promise of sodium-based batteries. Nature Reviews Materials, 6(11), 1020-1035.

42. Peng, J., Zhang, W., Liu, Q., Wang, J., Chou, S., Liu, H., & Dou, S. (2022). Prussian Blue analogues for sodium-ion batteries: past, present, and future. Advanced Materials, 34(15), 2108384.

43. Zhou, A., Cheng, W., Wang, W., Zhao, Q., Xie, J., Zhang, W., ... & Li, J. (2021). Hexacyanoferrate-type Prussian blue analogs: principles and advances toward high-performance sodium and potassium ion batteries. Advanced Energy Materials, 11(2), 2000943.

44. Jo, I. H., Lee, S. M., Kim, H. S., & Jin, B. S. (2017). Electrochemical properties of NaxMnFe (CN) 6· zH2O synthesized in a Taylor-Couette reactor as a Na-ion battery cathode material. Journal of Alloys and Compounds, 729, 590-596.

45. Yu, Z. E., Cheng, H., Lyu, Y., Liu, Y., Zhou, J., Chen, R., & Guo, B. (2021). A vacancy-free sodium manganese hexacyanoferrate as cathode for sodium-ion battery by high-salt-concentration preparation. *Journal of Alloys and Compounds*, *887*, 161388.

46. Deng, L., Qu, J., Niu, X., Liu, J., Zhang, J., Hong, Y., ... & Zhu, Y. (2021). Defect-free potassium manganese hexacyanoferrate cathode material for high-performance potassium-ion batteries. *Nature communications*, *12*(1), 2167.

47. El-Hady, D. A., Lyu, Y., Zhan, S., Yang, J., Wang, Y., Yang, F., ... & Shao, M. (2022). Vacancy and Composition Engineering of Manganese Hexacyanoferrate for Sodium-Ion Storage. *ACS Applied Energy Materials*, *5*(7), 8547-8553.

48. Song, J., Wang, L., Lu, Y., Liu, J., Guo, B., Xiao, P., ... & Goodenough, J. B. (2015). Removal of interstitial H2O in hexacyanometallates for a superior cathode of a sodium-ion battery. *Journal of the American Chemical Society*, *137*(7), 2658-2664.

49. Sottmann, J., Bernal, F. L., Yusenko, K. V., Herrmann, M., Emerich, H., Wragg, D. S., & Margadonna, S. (2016). In operando synchrotron XRD/XAS investigation of sodium insertion into the Prussian Blue Analogue Cathode material Na1. 32Mn [Fe (CN) 6] 0.83· z H2O. *Electrochimica Acta*, *200*, 305-313.

50. Deng, L., Qu, J., Niu, X., Liu, J., Zhang, J., Hong, Y., ... & Zhu, Y. (2021). Defect-free potassium manganese hexacyanoferrate cathode material for high-performance potassium-ion batteries. Nature communications, 12(1), 2167.

51. Xu, Y., Chang, M., Fang, C., Liu, Y., Qiu, Y., Ou, M., ... & Huang, Y. (2019). In situ FTIR-assisted synthesis of nickel hexacyanoferrate cathodes for long-life sodium-ion batteries. *ACS applied materials & interfaces*, *11*(33), 29985-29992.

52. Cheng, Q., Zhang, L., Lei, L., Huang, H., & Li, Y. (2022). Spectrophotometric Determination of Alkaline Phosphatase in Serum by A Copper Prussian Blue Analog as A Novel Polyphenol Oxidase-Like Nanozyme. *Analytical Letters*, 1-15.

53. Wu, X., Wu, C., Wei, C., Hu, L., Qian, J., Cao, Y., ... & Yang, H. (2016). Highly crystallized Na2CoFe (CN) 6 with suppressed lattice defects as superior cathode material for sodium-ion batteries. *ACS applied materials & interfaces*, *8*(8), 5393-5399.

54. Shen, Z., Guo, S., Liu, C., Sun, Y., Chen, Z., Tu, J., ... & Zhao, X. (2018). Na-rich Prussian white cathodes for long-life sodium-ion batteries. ACS Sustainable Chemistry & Engineering, 6(12), 16121-16129.

55. Jiang, M., Hou, Z., Wang, J., Ren, L., Zhang, Y., & Wang, J. G. (2022). Balanced coordination enables low-defect Prussian blue for superfast and ultrastable sodium energy storage. Nano Energy, 102, 107708.

56. Klewicki, J. K., & Morgan, J. J. (1998). Kinetic behavior of Mn (III) complexes of pyrophosphate, EDTA, and citrate. *Environmental Science & Technology*, *32*(19), 2916-2922.

57. Neale, Z. G., Liu, C., & Cao, G. (2020). Effect of synthesis pH and EDTA on iron hexacyanoferrate for sodium-ion batteries. Sustainable Energy & Fuels, 4(6), 2884-2891.

58. Tang, Y., Li, W., Feng, P., Zhou, M., Wang, K., Wang, Y., ... & Jiang, K. (2020). High-performance manganese hexacyanoferrate with cubic structure as superior cathode material for sodium-ion batteries. *Advanced Functional Materials*, *30*(10), 1908754.

59. Peng, F., Yu, L., Gao, P., Liao, X. Z., Wen, J., He, Y. S., ... & Ma, Z. F. (2019). Highly crystalline sodium manganese ferrocyanide microcubes for advanced sodium ion battery cathodes. Journal of Materials Chemistry A, 7(39), 22248-22256.

60. Yang, Y., Liu, E., Yan, X., Ma, C., Wen, W., Liao, X. Z., & Ma, Z. F. (2016). Influence of structural imperfection on electrochemical behavior of Prussian blue cathode materials for sodium ion batteries. Journal of The Electrochemical Society, 163(9), A2117.

61. Shibazaki, Y., Yamada, R., Saida, J., Kono, Y., Wakeda, M., Itoh, K., ... & Kimoto, K. (2020). High-pressure annealing driven nanocrystal formation in Zr50Cu40Al10 metallic glass and strength increase. *Communications Materials*, *1*(1), 53.

62. Hua, J., Deng, X., Niu, C., Huang, F., Peng, Y., Li, W., ... & Cheng, Y. B. (2020). A pressure-assisted annealing method for high quality CsPbBr 3 film deposited by sequential thermal evaporation. RSC advances, 10(15), 8905-8909.

63. Zhou, Q., Wang, L., Li, W., Zeng, S., Zhao, K., Yang, Y., ... & Sun, X. (2021). Carbon-decorated Na3V2 (PO4) 3 as ultralong lifespan cathodes for high-energy-density symmetric sodium-ion batteries. ACS Applied Materials & Interfaces, 13(21), 25036-25043.

64. Li, Y., Lam, K. H., & Hou, X. (2021). Reactant concentration and aging-time-regulated potassium manganese hexacyanoferrate as a superior cathode for sodium-ion batteries. *ACS Applied Energy Materials*, *4*(11), 13098-13109.

Appendix A. Supporting Materials for Chapter 2

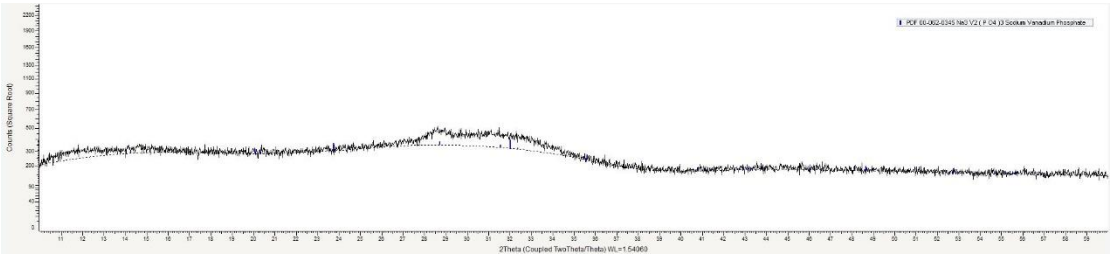

Figure A1 XRD diagram of materials before annealing process